Processing of Standard MR Images Prior Execution of the MR-Based Electrical Properties Tomography (MREPT) Method

Luis F. Díaz Rondón and Jan Tesarik

Abstract

Magnetic resonance-based electrical properties tomography (MREPT), uses information of the B_1^+ field distribution in MRI, and computes electrical properties relative permittivity and electrical conductivity via the Helmholtz equation. The method can be done using standard MRI sequences, boosting the method into a more realistic clinical environment. MRI images need to undergo certain image pre-processing to correct ailments like noise and phase shifting. Recent publications on the topic report encouraging results and give a detailed explanation on the theory in which the process is based. However, little or none explanation is given to the processing to which the standard MRI images need to undergo in order for the method to be correctly implemented. Emphasis will be put on processing and corrections that needed to be applied to the retrieved MRI images to arrive to the results that are here reported.

Keywords

MREPT • Electrical properties • Relative permittivity Electrical conductivity • In vivo • MRI

1 Introduction

Electrical properties for biological tissues can be computed in vivo using MR imaging if the B_1^+ field distribution in the scanned sample is determined. MREPT is a technique that is able to map relative permittivity (ε_r) and electrical conductivity (σ) via the Helmholtz equation [2]. Standard MRI sequences, Gradient Recalled Echo (GRE) low-flip-angle and Spin Echo (SE), can be used to derive a complex field distribution approximation [5]:

$$\sqrt{B_1^+ B_1^-} \rightarrow \sqrt{|I_{GRE}|} \cdot exp(\frac{1}{2}\measuredangle I_{SE}). \tag{1}$$

$$\varepsilon_r = -\frac{1}{\omega^2 \mu_0 \varepsilon_0} Re\left\{\frac{\nabla^2 \sqrt{B_1^+ B_1^-}}{\sqrt{B_1^+ B_1^-}}\right\}, \tag{2}$$

$$\sigma = \frac{1}{\omega \mu_0} Im\left\{\frac{\nabla^2 \sqrt{B_1^+ B_1^-}}{\sqrt{B_1^+ B_1^-}}\right\}, \tag{3}$$

In Eq. (1), $|I_{GRE}|$ stands for image intensity of the magnitude image from a GRE sequence with low flip angle; $\measuredangle I_{SE}$ stands for image intensity of the phase image of a SE sequence; and ω is the Larmor frequency. Equations (2) and (3) solve for relative permittivity and electrical conductivity respectively [5].

An experiment was done in which three liquid samples, enclosed in 250 ml plastic containers, with varying electrical properties, underwent MREPT following procedures previously published by other research groups. The results of this experiment were published in [3]. During this, some difficulties were encountered that were not covered in much detail in other publications and thus the reason for this document. Here will be covered the processing steps on the GRE and SE resulting images that took place in order achieve the satisfactory results reported on [3].

2 Pre-processing Prior MREPT

The scans were made on a 3T SIEMENS MRI scanner. From the scanner, all images were exported as DICOMS and imported into, and processed using MATLAB (MathWorks, USA).

L. F. Díaz Rondón (✉) · J. Tesarik
Faculty of Biomedical Engineering, Czech Technical University in Prague, Prague, Czech Republic
e-mail: diazluis@fbmi.cvut.cz

L. Lhotska et al. (eds.), *World Congress on Medical Physics and Biomedical Engineering 2018*,
IFMBE Proceedings 68/3, https://doi.org/10.1007/978-981-10-9023-3_142

2.1 GRE Low-Flip-Angle Magnitude

Square root The magnitude image coming from the low-flip-angle GRE sequence undergoes a simple square root operation yielding the magnitude term of the complex number seen in Eq. (1). A filtering stage is necessary to proceed. Getting rid of the noise in the image gave a considerable amount of trouble, as different filtering options, normally used in image processing, were applied with no satisfactory results. Noise needs to be filtered out in such subtle way as to conserve the data which in this case, is supposed to represent the magnitude values in space of the RF magnetic field distribution. Figure 1a shows the original magnitude image coming from the GRE sequence, while the square-rooted GRE can be seen on Fig. 1c.

De-noise The taken approach was the wavelet transform. By using a basic built-in de-noising function in Matlab (MathWorks, USA) [6], it was possible to reduce the noise in the image at such point that real results matched the expectations. Figure 2d and e show the surface of one scanned sample before and after the wavelet de-noising function.

2.2 SE Phase

Re-scaling SIEMENS displays phase images using intensity values from a scale of 0 to 4096, with 2048 being the zero phase. The image needs to be operated in such way that it could be re-scaled from (π) to ($-\pi$). Figure 1e shows original phase image from SE, and Fig. 1f, the image after re-scaling.

Phase correction SE phase images, may come with offset and spatially varying errors, known as zero-order and first-order phase errors. In [1], a very simple and effective method for first- and zero-order phase correction is very well explained, and this was the one successfully applied during the experiments. This method starts by stating that the image intensity from SE image is expressed by

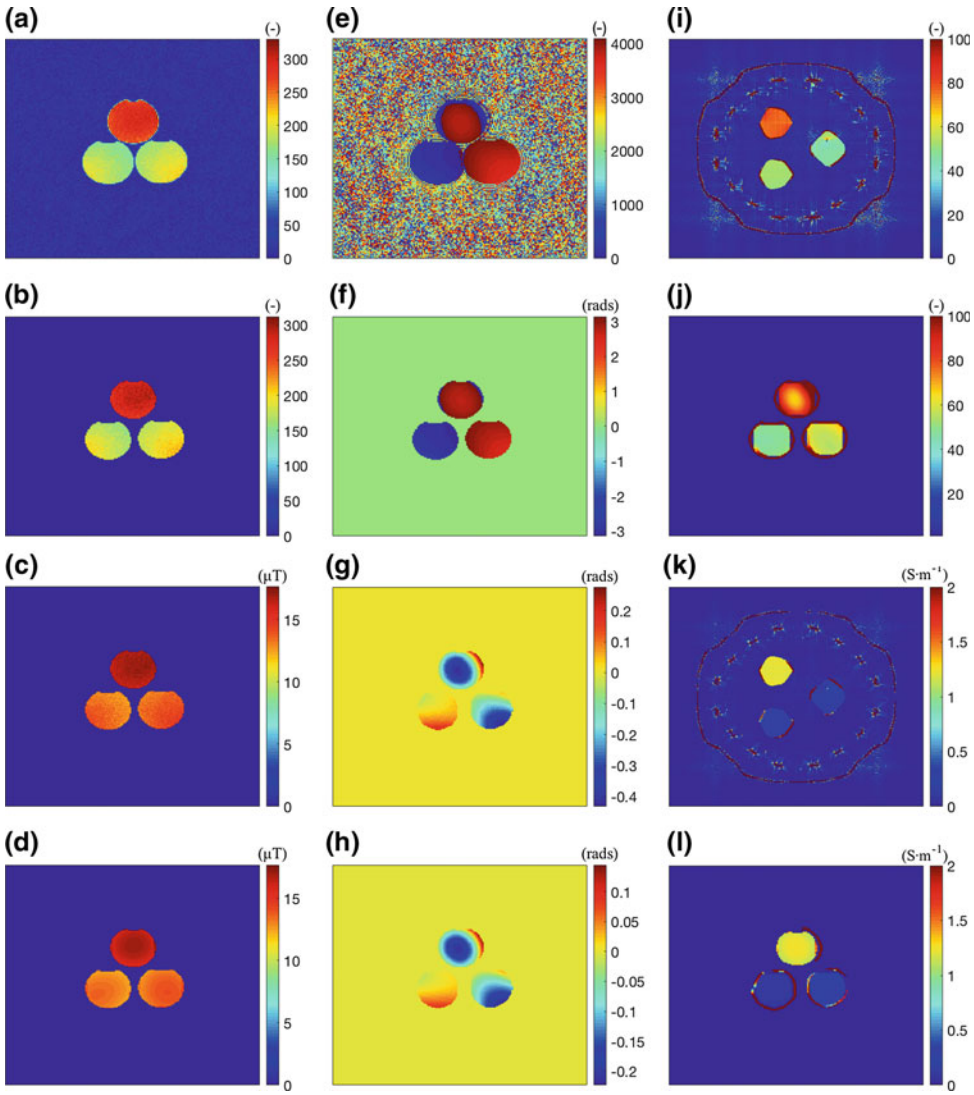

Fig. 1 Resulting images from the different stages of their processing. **a** Original GRE low-flip-angle magnitude image. **b** GRE low-flip-angle image with background noise removed and edges extracted. **c** GRE magnitude square-rooted. **d** Square-root of GRE low-flip-angle surface fitted. **e** Original SE phase image. **f** SE phase image, re-scaled from (π, $-\pi$), with background noise removed and edges extracted. **g** SE phase-corrected. **h** Half of SE phase-corrected surface-fitted. **i** ε_r map (numerical simulations). **j** ε_r map (MREPT). **k** σ map (numerical simulations). **l** σ map (MREPT)

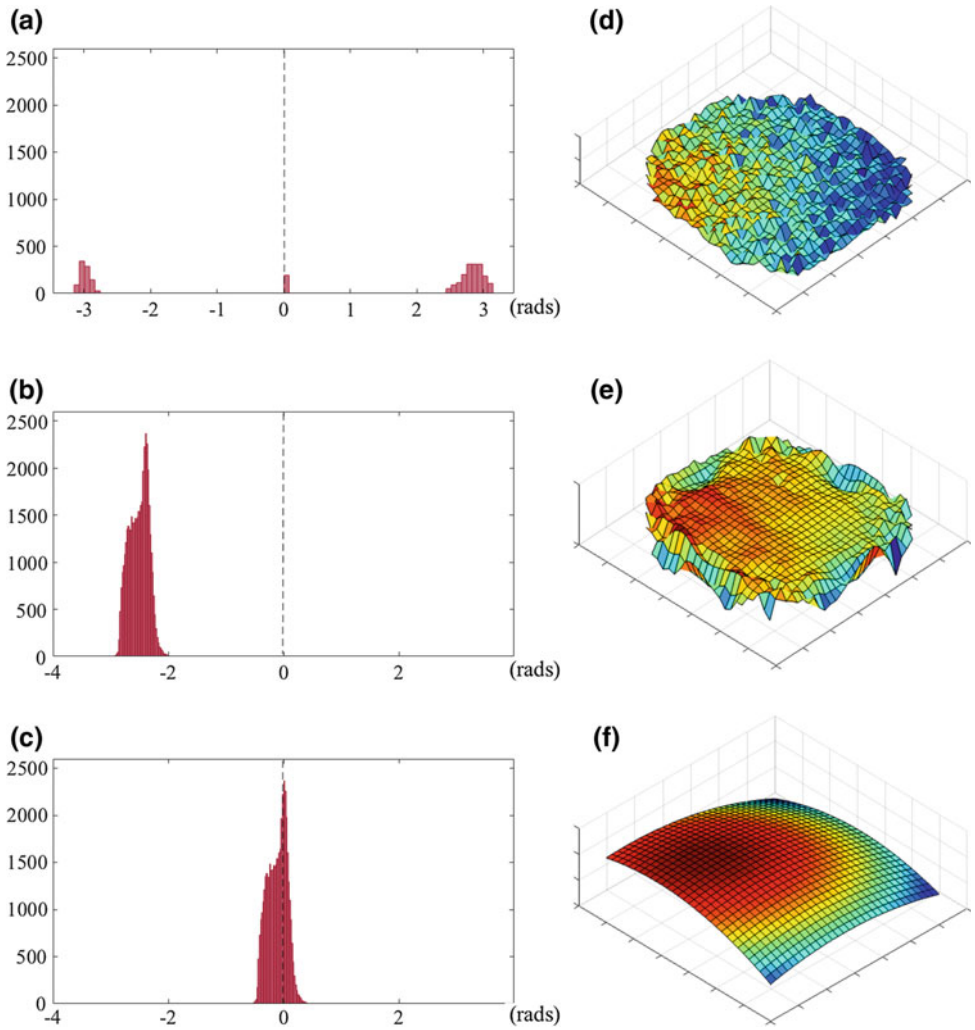

Fig. 2 **a** Histogram: SE phase values distribution from original re-scaled SE phase image. **b** Histogram: SE phase values distribution after first-order phase correction. **c** Histogram: SE phase values distribution after first-order and zero-order phase correction. **d** Noisy surface from a sample in square-rooted GRE magnitude image. **e** Sample's surface from square-rooted GRE magnitude image after wavelet transform de-noising. **f** Sample's surface from de-noised square-rooted GRE magnitude image after fitting

$$\hat{f}(x,y) = f(x,y)exp^{i\phi_0}exp^{i\epsilon_1 x},$$

where ϕ_0 is the zero-order phase error, ϵ_1 the first-order phase error, and $f(x,y)$ is the true image intensity. These two error terms are determined using an autocorrelation function and histogram operations, and then by inverse multiplication the error terms are cancelled. In Fig. 2a–c can be seen how the phase values are distributed in the image, at the beginning, after first-order error is corrected, and after zero-order error is corrected. Figure 1g shows SE phase image after successful phase correction. After the correction, the phase image can then be multiplied by 0.5 (Fig. 1h), following Eq. (1).

2.3 Surface Fitting

Computation of the Laplacian in a 2D or 3D image can be easily done by convolution using the appropriate kernel. Problem resides in noisy images and also in kernel position, as edges may be inside a different tissue type, increasing noise and/or giving out false information. In order to deal with this issue, mainly the noise, a surface fitting took place. Every surface of the samples were extracted from the original image, and individually underwent a second-order polynomial surface-fit (Fig. 2f), following a parabola-fitting approach suggested and applied in [4]. Once all surfaces, from the magnitude and phase images were fitted, they were inserted back into their original format. End results can be seen on Fig. 1d and h. Done this, all needed to satisfy the equations and solve for relative permittivity and electrical conductivity, was to join square-rooted de-noised-surface-fitted GRE magnitude image, and halved phase-corrected surface-fitted SE phase image, into a complex-valued matrix, following Eq. (1).

2.4 MREPT and Resulting Electrical Properties

For every pixel, electrical properties were computed using Eqs. (2) and (3). Resulting images can be seen on Fig. 1j and l, for relative permittivity map and electrical

Table 1 Mean values of electrical properties of liquid samples: real values, results from numerical simulations, and results from MREPT

Sample #	Real		Sims.		MREPT	
	$\varepsilon_r(-)$	$\sigma(\mathrm{S}\cdot\mathrm{m}^{-1})$	$\varepsilon_r(-)$	$\sigma(\mathrm{S}\cdot\mathrm{m}^{-1})$	$\varepsilon_r(-)$	$\sigma(\mathrm{S}\cdot\mathrm{m}^{-1})$
1	73.9	1.24	76.9	1.22	75.5	1.27
2	48.1	0.17	44.9	0.17	48.3	0.11
3	53.7	0.34	52.2	0.33	56.6	0.34

conductivity map respectively. Figure 1i and k are correspondent electrical properties maps resulting from numerical simulations [3] (Table 1).

3 Conclusion

Magnetic Resonance-based Electrical Properties Tomography manages to provide a closer look into mapping of electrical properties of biological tissues in vivo. For those that are interested in following in this line of research it is important to understand that processing of delivered MR images is necessary, and its complexity will depend on the complexity of the imaged tissue.

Acknowledgements This research has been supported by the research program of the Czech Science Foundation, Project no. 17-00477Y, Physical nature of interactions of EM fields generated by MTM structures with human body and study of their prospective use in medicine.

References

1. Ahn, C.B., Cho, Z.H.: A New Phase Correction Method in NMR Imaging Based on Autocorrelation and Histogram Analysis. IEEE Transactions on Medical Imaging **6**(1), 32–36 (1987). https://doi.org/10.1109/tmi.1987.4307795
2. Bulumulla, S.B., Lee, S.K., Yeo, D.T.B.: Conductivity and permittivity imaging at 3.0T. Concepts in magnetic resonance. Part B, Magnetic resonance engineering **41B**(1), 13–21 (2012). https://doi.org/10.1002/cmr.b.21204
3. Diaz, L.F., Vrba, J., Vrba, D.: Extraction of electrical properties of strokes from magnetic resonance scans - testing on simplified head phantoms. PIERS - Progress in Electromagnetics Research Symposium, Singapoor (2017)
4. Katscher, U., Djamshidi, K., Voigt, T., Ivancevic, M., Abe, H., Newstead, G., Keupp, J.: Estimation of Breast Tumor Conductivity Using Parabolic Phase Fitting. In: ISMRM 20th Annual Meeting, Melbourne, vol. 20, p. 3482. ISMRM (2012)
5. Lee, S.K., Bulumulla, S., Lamb, P., Hancu, I.: Measurement of electrical properties of biological tissue at radio frequencies using magnetic resonance imaging. In: 2015 9th European Conference on Antennas and Propagation (EuCAP), pp. 1–4 (2015)
6. MathWorks: Understanding waveletes. URL https://www.mathworks.com/videos/series/understanding-wavelets-121287.html